

UC Davis

UC Davis Previously Published Works

Title

Multiparametric MRI model with dynamic contrast-enhanced and diffusion-weighted imaging enables breast cancer diagnosis with high accuracy.

Permalink

<https://escholarship.org/uc/item/2dn3h29w>

Journal

Journal of Magnetic Resonance Imaging, 49(3)

Authors

Zhang, Michelle
Horvat, Joao
Bernard-Davila, Blanca
et al.

Publication Date




2019-03-01

DOI

10.1002/jmri.26285

Peer reviewed

Multiparametric MRI Model With Dynamic Contrast-Enhanced and Diffusion-Weighted Imaging Enables Breast Cancer Diagnosis With High Accuracy

Michelle Zhang, MD,¹ Joao V. Horvat, MD,¹ Blanca Bernard-Davila, MPH, MS,¹ Maria Adele Marino, MD,^{1,2}  Doris Leithner, MD,^{1,3} R. Elena Ochoa-Albiztegui MD,¹ Thomas H. Helbich, MD,^{4*} Elizabeth A. Morris, MD,¹ Sunitha Thakur, PhD,¹  and Katja Pinker, MD, PhD^{1,4} 

Background: The MRI Breast Imaging-Reporting and Data System (BI-RADS) lexicon recommends that a breast MRI protocol contain T₂-weighted and dynamic contrast-enhanced (DCE) MRI sequences. The addition of diffusion-weighted imaging (DWI) significantly improves diagnostic accuracy. This study aims to clarify which descriptors from DCE-MRI, DWI, and T₂-weighted imaging are most strongly associated with a breast cancer diagnosis.

Purpose/Hypothesis: To develop a multiparametric MRI (mpMRI) model for breast cancer diagnosis incorporating American College of Radiology (ACR) BI-RADS recommended descriptors for breast MRI with DCE, T₂-weighted imaging, and DWI with apparent diffusion coefficient (ADC) mapping.

Study Type: Retrospective.

Subjects: In all, 188 patients (mean 51.6 years) with 210 breast tumors (136 malignant and 74 benign) who underwent mpMRI from December 2010 to September 2014.

Field Strength/Sequence: IR inversion recover DCE-MRI dynamic contrast-enhanced magnetic resonance imaging VIBE Volume-Interpolated-Breathhold-Examination FLASH turbo fast-low-angle-shot TWIST Time-resolved angiography with stochastic Trajectories.

Assessment: Two radiologists in consensus and another radiologist independently evaluated the mpMRI data. Characteristics for mass ($n = 182$) and nonmass ($n = 28$) lesions were recorded on DCE and T₂-weighted imaging according to BI-RADS, as well as DWI descriptors. Two separate models were analyzed, using DCE-MRI BI-RADS descriptors, T₂-weighted images, and ADCmean as either a continuous or binary form using a previously published ADC cutoff value of $\leq 1.25 \times 10^{-3}$ mm²/sec for differentiation between benign and malignant lesions. Histopathology was the standard of reference.

Statistical Tests: χ^2 test, Fisher's exact test, Kruskal-Wallis test, Pearson correlation coefficient, multivariate logistic regression analysis, Hosmer-Lemeshow test of goodness-of-fit, receiver operating characteristics analysis.

Results: In Model 1, ADCmean ($P = 0.0031$), mass margins with DCE ($P = 0.0016$), and delayed enhancement with DCE ($P = 0.0016$) were significantly and independently associated with breast cancer diagnosis; Model 2 identified ADCmean ($P = 0.0031$), mass margins with DCE ($P = 0.0012$), initial enhancement ($P = 0.0422$), and delayed enhancement with DCE ($P = 0.0065$) to be significantly independently associated with breast cancer diagnosis. T₂-weighted imaging variables were not included in the final models.

View this article online at wileyonlinelibrary.com. DOI: 10.1002/jmri.26285

Received May 14, 2018, Accepted for publication Jul 23, 2018.

*Address reprint requests to: T.H.H., Medical University of Vienna, Department of Biomedical Imaging and Image-guided Therapy, Division of Molecular and Gender Imaging, Vienna, Austria. E-mail: thomas.helbich@meduniwien.ac.at

From the ¹Memorial Sloan Kettering Cancer Center, Department of Radiology, Breast Imaging Service, NY, New York, USA; ²Medical University of Vienna, Department of Biomedical Imaging and Image-guided Therapy, Division of Molecular and Gender Imaging, Vienna, Austria; ³University Hospital Frankfurt, Department of Diagnostic and Interventional Radiology, Frankfurt, Germany; and ⁴Department of Biomedical Sciences and Morphologic and Functional Imaging, University of Messina, Messina, Italy

Additional supporting information may be found in the online version of this article.

This is an open access article under the terms of the Creative Commons Attribution-NonCommercial License, which permits use, distribution and reproduction in any medium, provided the original work is properly cited and is not used for commercial purposes.

Data Conclusion: mpMRI with DCE-MRI and DWI with ADC mapping enables accurate breast cancer diagnosis. A model using quantitative and qualitative descriptors from DCE-MRI and DWI identifies breast cancer with a high diagnostic accuracy. T₂-weighted imaging does not significantly contribute to breast cancer diagnosis.

Level of Evidence: 3

Technical Efficacy: Stage 2

J. MAGN. RESON. IMAGING 2019;49:864–874.

Dynamic contrast-enhanced magnetic resonance imaging (DCE-MRI) of the breast is the most sensitive test for breast cancer, with a pooled sensitivity of 93% and outperforms mammography, digital breast tomosynthesis, and ultrasound in women at any given risk of breast cancer.^{1–4} However, due to an overlap of morphologic and kinetic features between benign and malignant lesions, there are limitations in specificity (pooled specificity 71%) leading to unnecessary breast biopsies.^{5,6} To improve specificity, several other MRI techniques such as diffusion-weighted imaging (DWI), proton MR, and phosphorus spectroscopy and sodium imaging have been explored, with DWI having emerged as the most robust and valuable for an improved differentiation of benign and malignant breast lesions.^{5,7–13} In DWI, the random movement of water molecules in body tissue, ie, Brownian motion, can be visualized and quantified by calculating the apparent diffusion coefficient (ADC) value. Breast cancer typically shows restricted water molecule diffusivity with high signal on DWI and lower signal on ADC maps due to increased cell density, compression of the extracellular space, and microstructural changes.^{11,14}

Multiple studies have demonstrated that multiparametric (mp) MRI of the breast using DCE-MRI and DWI significantly improves the diagnostic accuracy in breast cancer and may reduce unnecessary breast biopsies of benign lesions.^{15–19} The American College of Radiology (ACR) Breast Imaging-Reporting and Data System (BI-RADS) MRI lexicon provides "standardized breast imaging terminology, report organization, assessment structure, and a classification system for mammography, ultrasound, and MRI of the breast."²⁰ For MRI of the breast, thus far it provides morphological and functional descriptors for DCE-MRI and T₂-weighted imaging—these constitute the typical breast MRI protocol—as well as recommendations for their combined analysis with the aim to assign, based on all descriptors, a final BI-RADS classification, which determines the probability of malignancy of a lesion.²⁰ Given the compelling improvements in diagnostic accuracy that are afforded with mpMRI when using both DCE-MRI and DWI, it is important that DWI is integrated into the MRI BI-RADS lexicon. However, it remains unclear what is the contribution of the individual BI-RADS descriptors from DCE-MRI, T₂-weighted imaging, as well as different ADC metrics in this context and whether all are necessary for an accurate breast cancer diagnosis. Therefore, we aimed to develop mpMRI models for the differentiation of benign and malignant breast tumors based on the ACR BI-RADS-recommended

descriptors for breast mpMRI using T₂-weighted imaging, DCE, and DWI with ADC mapping.

Materials and Methods

The local Institutional Review Board of our hospital approved this prospective single-institution study (EK 510/2009) and retrospective data analysis. The research was performed in accordance with relevant guidelines/regulations and we obtained informed consent from all patients.

Patient Population

A research database was searched for patients who underwent breast MRI including T₂-weighted, DCE-MRI, and DWI sequences per international recommendations²¹ between December 2010 and September 2014, and fulfilled the following inclusion criteria: 18 years or older, not pregnant or breastfeeding, suspicious finding at mammography or breast ultrasonography (BI-RADS 4 or 5), no previous breast cancer treatment, no high-risk patients (>20% lifetime risk of breast cancer), and no contraindications for MRI or MRI contrast agents. Patients were excluded if there was no histopathologic confirmation by either image-guided or surgical biopsy available or if the MR images demonstrated severe motion or susceptibility artifacts.

In all, 210 lesions in 188 patients were identified using the selection criteria of lesion size ≥ 5 mm and a distribution of at least one-third benign lesions. Electronic medical records were reviewed and the following patient characteristics were recorded for each patient: age at imaging and detailed histopathology including tumor grade, receptor status, and molecular subtypes for malignant lesions.

MRI Technique

Patients underwent breast MRI in the prone position using a 3T scanner (Tim Trio, Siemens, Erlangen, Germany) utilizing a four-channel breast coil (InVivo, Orlando, FL). The MRI protocol included following sequences:

- 1). A T₂-weighted turbo spin echo sequence with fat suppression: repetition time / echo time (TR/TE) = 4800/9 msec; field of view (FOV) 340 mm; 48 slices at SI 3 mm; flip angle 128°; matrix 384 × 512; time of acquisition (TA): 2 min 16 sec.
- 2). DWI three-acquisition trace diffusion-weighted, double-refocused, single-shot echo-planar imaging with inversion recovery fat suppression: TR/TE/TI 8000/59/210 msec; FOV 360 × 202 mm; 24 slices at 5 mm; matrix 172 × 96 (50% oversampling); b-values 50 and 850 s/mm²; TA 2 min 56 sec.
- 3). DCE-MRI: i) From December 2010 to December 2011, a split protocol with the following parameters was used: T₁-

TABLE 1. Imaging Characteristics Assessed on DCE-MRI

BI-RADS descriptors		Categories/explanation
Mass	Shape	Round, oval, irregular
	Margin	Circumscribed, irregular, spiculated
	Internal enhancement characteristics	Homogeneous, heterogeneous, rim enhancement, dark internal septations
NME	Distribution	Focal, linear, segmental, regional, multiple regions, diffuse
	Internal enhancement pattern	Homogeneous, heterogeneous, clumped, clustered ring
	Symmetry	Symmetric, asymmetric
Kinetic curve (on DCE)	Initial phase	Slow, medium, fast
	Delayed phase	Persistent, plateau, washout
T2 characteristics	Signal	Hypointense, isointense, hyperintense
	Peri-tumoral edema	Yes, no

DCE = dynamic contrast-enhanced; NME = nonmass enhancement.

weighted volume-interpolated-breathhold-examination (VIBE) sequences (TR/TE 3.62/1.4 msec; FOV 320 mm; 72 slices; 1.7 mm isotropic; matrix 192×192 ; one average; 13.2 sec per volume) and T_1 -weighted turbo fast-low-angle-shot-3D sequences with selective water-excitation (TR/TE 877/3.82 msec; FOV 320 mm; 96 slices; 1 mm isotropic; matrix 320×134 ; on average; TA 2 min) with a total TA of 9 min 20 sec; (ii) From December 2011 to September 2014, transversal T_1 -weighted time-resolved angiography with stochastic trajectories (TWIST) with water excitation fat-saturation was used: TR/TE 6.23/2.95 msec; flip angle 15° , FOV $196 \times 330 \text{ mm}^2$; 144 slices; spatial resolution $0.9 \times 0.9 \times 1 \text{ mm}$; temporal interpolation factor 2; temporal resolution 14 sec; matrix 384×384 ; one average; center k -space region with a resampling rate of 23%; reacquisition density of peripheral k -space 20%; TA 6 min 49 sec.

A standard dose (0.1 mmol/kg body-weight) of gadotaremeglumine (Gd-DOTA; Dotarem, Guerbet, France) was injected intravenously as a bolus at 4 ml/s with a saline flush after injection. MRI examination time was 12–16 minutes.

Imaging Analysis

DCE and DWI MRI data were evaluated by two breast radiologists in consensus (reader 1: >12 years of experience, reader 2: 5 years of experience) and again by two readers independently (reader 1: >12 years of experience, reader 3: 4 years of experience). All readers were aware that the patients had a breast lesion but were not provided with the previous imaging or histopathological results.

DCE-MRI. For both models, DCE-MRI data were evaluated using the 5th edition ACR MRI BI-RADS lexicon.²⁰ Location and laterality of the lesion were recorded. On DCE, lesions were categorized as mass or nonmass enhancement (NME) and classified according to BI-RADS. In addition, signal intensity on T_2 -weighted sequences and the presence or absence of a peritumoral edema was noted. For analysis of lesion enhancement kinetics, 2D regions of interest (ROIs), which were manually drawn, were placed in the most enhancing part of a lesion and an automated semiquantitative curve-type analysis was performed using dedicated software, ie, the DCE Tool plugin v2.2 for OSIRIX software.²² Average lesion sizes on DCE-MRI were determined. All recorded BI-RADS descriptors with DCE-MRI and T_2 -weighted imaging are summarized in Table 1.

DWI. High b-value (ie, 850 s/mm^2) images were qualitatively assessed for hyperintense regions corresponding to the lesion on DCE-MRI. The slice with the greatest representative portion of the tumor was selected. One 2D ROI with a minimum area of 10 mm^2 was drawn on the part of the tumor with the lowest ADC and another larger 2D ROI around the whole tumor was using OSIRIX software.²² For the small ROI, the mean ADC (ADC_{mean}) was recorded, and for the large ROI, the minimum ADC (ADC_{min}) and maximum ADC (ADC_{max}) were recorded; these were used as variables in model development (see Statistical Analysis section, below).

TABLE 2. Imaging Characteristics Assessed on DWI/ADC

Imaging characteristics	Categories/explanation
ADC mean	Mean ADC with the ROI drawn over the part of the lesion with the visually lowest ADC
ADC min	Minimum ADC with the ROI drawn over the entire lesion
ADC max	Maximum ADC with the ROI drawn over the entire lesion
DWI signal on b50	Isointense, hyperintense
DWI signal pattern on b850	Homogeneous, heterogeneous, rim

ADC = apparent diffusion coefficient; DWI = diffusion-weighted imaging; ROI = region of interest.

Lesion signal intensity on the b50 DW images as either iso- or hyperintense was recorded. DWI signal pattern was classified as homogenous, heterogeneous, or rim appearance. The recorded DWI variables are summarized in Table 2.

Histopathology

Histopathology was used as the standard of reference. Histopathologic diagnosis was established by one experienced pathologist using either image-guided needle biopsy or surgical specimens. In the case of a benign histopathological diagnosis at image-guided needle biopsy, the final diagnosis was benign. In the case of a high-risk lesion with uncertain potential for malignancy, the final diagnosis was established with open surgery.

Statistical Analysis

Statistical analysis was performed by a statistician using SAS, v9.4 (SAS Institute, Cary, NC). All calculations were performed on a per-lesion basis. The main outcome was presence of malignancy. We dichotomized disease status as positive or negative for malignancy using histopathology as the standard of reference. Variables that were dichotomized included: peritumoral edema in T₂-weighted imaging (present vs. absent), signal intensity in DWI b50 (iso- vs. hyperintense), mass internal enhancement characteristics (homogenous/dark internal septations vs. heterogeneous/rim enhancement), and initial enhancement (slow/medium vs. fast). Additional binary variables included laterality (right, left). DWI signal pattern (homogenous, heterogeneous, rim), shape (round, oval, irregular) and margins (circumscribed, irregular, spiculated) for masses, and delayed phase enhancement (persistent, plateau, wash-out) were examined as 3-level categorical variables. Age, ADCmin, ADCmax were kept in

continuous form. DWI ADCmean was examined in both its continuous and binary form. DWI ADC (continuous) was log-transformed to approximate the normal distribution.

Variables of patients with benign lesions and those with malignant lesions were compared using the χ^2 test, Fisher's exact test, or the Kruskal–Wallis test for categorical variables, as appropriate. In a preliminary analysis, evaluation of the linear relationship between clinically related variables was calculated using the Pearson correlation coefficient. Collinearity among the predictor variables was detected (tolerance threshold $r \leq 0.7$). Variables that did not have correlation coefficient values within the tolerance threshold were excluded from the model. Table 3 summarizes the covariates for inclusion in the model. A multivariate logistic regression analysis was performed to determine parameters that jointly are associated with malignancy.

Two separate models were analyzed, using ADCmean as either a continuous or binary form using a previously published ADC cut-off value of $\leq 1.25 \times 10^{-3} \text{ mm}^2/\text{sec}^{23}$ for differentiation between benign and malignant lesions. ADCmean as a continuous form was log-transformed to approximate the normal distribution. All models considered the same covariates for inclusion (Table 3). Covariates were removed from the multivariate model using forward selection. The Hosmer–Lemeshow test of goodness-of-fit was performed to examine model calibration. Discriminative ability was examined

TABLE 3. Covariates Included in the Logistic Regression Model

Covariates / Predictor of presence of disease	Univariate analysis (P-value)
Age	$P < 0.0001$
Laterality	$P = 0.0086$
ADC max	$P < 0.0001$
ADC mean ^{ab}	$P < 0.0001$
ADC min	$P < 0.0001$
DWI signal on b50	$P = 0.0427$
T2 peritumoral edema	$P < 0.0001$
DCE kinetic initial phase ^b	$P < 0.0001$
DCE kinetic delayed phase ^{a,b}	$P < 0.0001$
Mass shape	$P < 0.0001$
Mass margin ^{a,b}	$P < 0.0001$
DCE internal enhancement	$P < 0.0001$

ADC = apparent diffusion coefficient; DCE = dynamic contrast-enhanced; DWI = diffusion-weighted imaging.

^aSignificantly associated with breast cancer diagnosis and included in Model 1.

^bSignificantly associated with breast cancer diagnosis and included in Model 2.

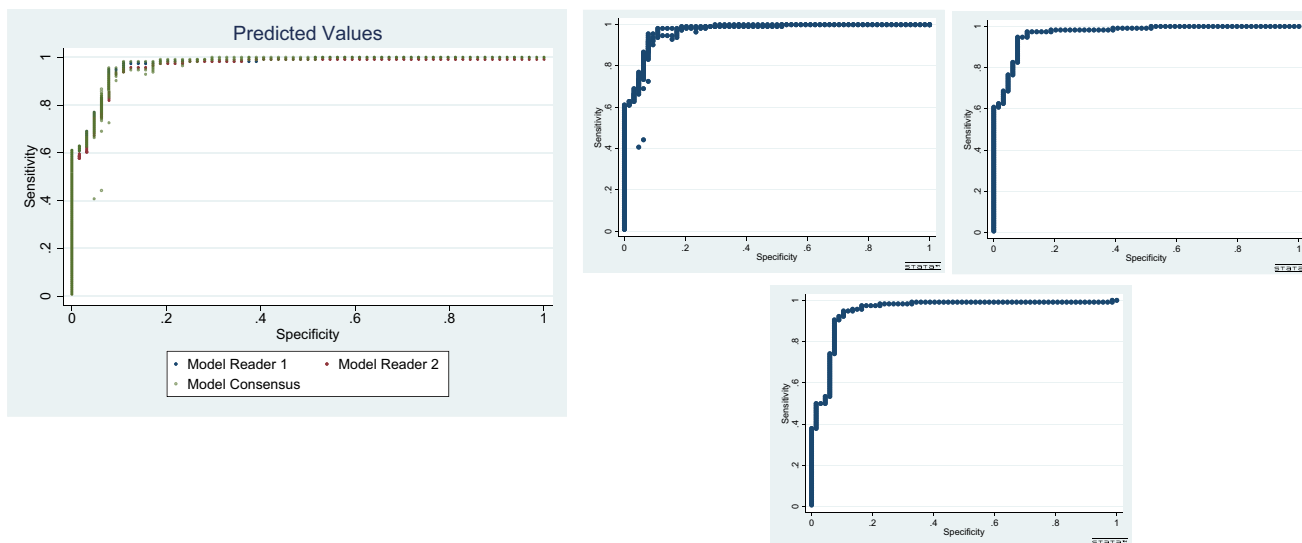


FIGURE 1: Scatterplots of computed predicted values from previously fitted consensus data evaluated against predictive values generated for new independent reader observations.

using the area under the receiver operating characteristics (ROC) curve (AUC).²⁴ Statistical significance was assigned for $P < 0.05$.

Computed predicted values from previously fitted consensus data were evaluated against predictive values generated for new independent reader observations. Predicted values were calculated for independent readers (reader 1, reader 3) and compared to the initial consensus model (Model 2). The results indicate that the predicted probabilities for each individual reader model are consistent with the consensus data (Fig. 1).

Results

Patients

Table 4 summarizes histopathological diagnoses of the patients included in our study. There were 74 benign and 136 malignant lesions in 188 patients (mean 51.6 years,

range 21–86); among the patients, 16 had multiple or bilateral lesions. Of the 210 lesions in total, there were 182 masses (116 malignant and 66 benign) and 28 NME masses (20 malignant, 8 benign) as defined according to the MRI BI-RADS lexicon. The overall average lesion size was 27 mm (range 6–100). Malignant lesions had a larger average lesion size (30.6 mm) compared with benign lesions (21.4 mm).

On DWI, malignant lesions showed significant lower average ADCmean ($0.90 \times 10^{-3} \text{ mm}^2/\text{sec}$) compared with benign lesions ($1.43 \times 10^{-3} \text{ mm}^2/\text{sec}$) ($P < 0.0001$).

On DCE-MRI, DCE morphological features associated with breast cancer presenting as masses were irregular shape, irregular/spiculated margin, and heterogeneous/rim internal enhancement pattern ($P < 0.0001$, Table 5). DCE morphological features associated with breast cancer presenting as

TABLE 4. Histopathological Subtypes of the Patient Population

Histology	Subtype	<i>n</i>	%
Malignant (<i>n</i> = 136)	Invasive ductal carcinoma	119	56.6
	Invasive lobular carcinoma	10	4.8
	Ductal carcinoma in situ	4	1.9
	Mucinous	1	0.5
	Myelosarcoma Metastasis	1	0.5
Benign (<i>n</i> = 74)	High risk lesions	9	4.3
	Fibroadenoma / fibroadenomatoid hyperplasia	47	22.4
	Fibrocystic changes without atypia ^b	12	5.7
	Miscellaneous (eg, fat necrosis, cyst with inflammation)	5	2.4
Total		210	100

TABLE 5. Distribution of T2-Weighted Imaging, BI-RADS DCE-MRI and Qualitative and Quantitative DWI Variables for Benign and Malignant Tumors

Total	Benign (n = 74)	Malignant (n = 136)	P-value
Lesion laterality			0.0086
right	45 (21.7)	58 (27.5)	
left	29 (13.5)	78 (37.2)	
Lesion size			<.0001
mean (SD)	21.4 (20.36)	30.6 (23.95)	
median(min-max)	15.0 (6-100)	30.6 (2-100)	
Mass shape			<0.0001
oval	17(9.4)	14(7.8)	
round	40(22.2)	21(11.7)	
irregular	8(4.4)	80(44.4)	
Mass margin			<0.0001
circumscribed	54(30.2)	8(4.5)	
irregular	6(3.4)	57(31.8)	
spiculated	4(2.2)	50(27.9)	
Mass internal enhancement characteristics			<0.0001
homogenous	29(16.1)	18(10.0)	
heterogeneous	18(10.0)	84(46.7)	
rim enhancement	0(0.0)	11(6.1)	
dark internal septations	19(36.7)	1(0.6)	
NME Distribution			0.0071
focal	6 (20.0)	5(16.7)	
regional	3(10.0)	9(30.0)	
segmental	0(0.0)	7(23.3)	
Internal enhancement pattern			0.003
homogenous	6(20.7)	3(10.3)	
heterogeneous	2(6.9)	16(55.2)	
clumped	NA	2(6.9)	
clustered ring	NA	NA	
DWI			
ADC mean (SD)	1433.4 (374.17)	902.9 (237.36)	<0.0001
ADC max (SD)	2133.4 (405.54)	2041.6(442.34)	<0.0001
ADC min (SD)	681.6 (481.57)	282.5 (306.86)	<0.0001
DWI_ADCmeanCAT			<0.0001

TABLE 5. Continued

Total	Benign (n = 74)	Malignant (n = 136)	P-value
<1.255 × 10 ⁻³ mm ² /s	24(11.4)	127(60.8)	
>1.255 × 10 ⁻³ mm ² /s	50(23.9)	9(4.3)	
Signal intensity b0			0.0427
isointense	34(16.3)	44(21.1)	
hyperintense	40(19)	92(44.0)	
DWI pattern b850			<0.0001
homogenous	53(25.2)	43(20.6)	
heterogeneous	19(9.1)	66(31.6)	
rim appearance	2(0.96)	27(12.9)	

^aHigh risk lesions includes: atypical ductal hypoplasia, sclerosing adenosis with atypia, metaplasia with atypia, metaplasia with atypia, complex sclerosing lesion, columnar cell changes with atypia.
^bFibrocystic changes include: ductal hyperplasia, columnar cell changes, focal fibrosis, sclerosing adenosis, apocrine metaplasia, fibrocystic changes.
 ADC = apparent diffusion coefficient; DWI = diffusion-weighted imaging; NME = nonmass enhancement.

NME cancers were regional/segmental distribution and heterogeneous/clumped internal enhancement pattern ($P < 0.0001$, Table 5). Frequent morphological features for benign breast lesions presenting as masses were round/oval shapes, circumscribed margins, and homogenous/dark septations internal enhancement pattern characteristics ($P < 0.0001$, Table 5). For benign breast lesions presenting as NME, the significant features were focal distribution and homogenous internal enhancement pattern ($P < 0.0001$, Table 5).

mpMRI Model 1 Using an ADCmean Cutoff

Here we used the previously published ADCmean cutoff of $\leq 1.25 \times 10^{-3} \text{ mm}^2/\text{sec}^{23}$ to identify MRI BI-RADS features that differentiate between benign and malignant tumors. Multivariate logistic regression analysis determined that ADCmean (binary) on DWI and margins and enhancement in the delayed phase on DCE-MRI were significantly associated with breast cancer diagnosis.

Following these findings, our mpMRI Model 1 incorporated ADCmean (binary) on DWI and margins and delayed enhancement pattern on DCE-MRI. Model 1 discriminated between benign and malignant breast tumors with an AUC of 0.952 (Fig. 2). The odds ratio (OR) of a lesion with ADCmean $< 1.25 \times 10^{-3} \text{ mm}^2/\text{sec}$ being a cancer was 8.9 (2.1–39.0) ($P < 0.0031$). Lesions with plateau or washout type delayed kinetic curve had a 4.3 greater odds of being malignant (OR = 4.320; confidence interval [CI] = 1.745–10.69) compared with those with persistent type kinetic curve significance ($P = 0.0016$). Lesions with

spiculated or irregular margins had 4.8 greater odds of being malignant (OR = 4.814; CI = 1.93–12.03) than lesions with circumscribed margins ($P = 0.0016$) (Figs. 3–4).

mpMRI Model 2 Using an ADCmean as a Continuous Variable

Here we used ADCmean as a continuous variable to identify MRI BI-RADS features that differentiate between benign and malignant tumors. Multivariate logistic regression analysis

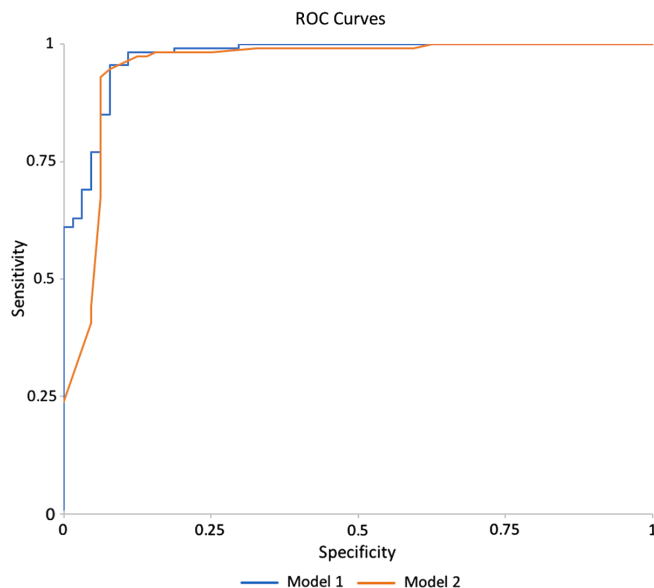


FIGURE 2: ROC of both mpMRI Model 1—using an ADCmean cutoff of $\leq 1.25 \times 10^{-3} \text{ mm}^2/\text{sec}$ and ROC mpMRI Model 2—using ADCmean as a continuous variable

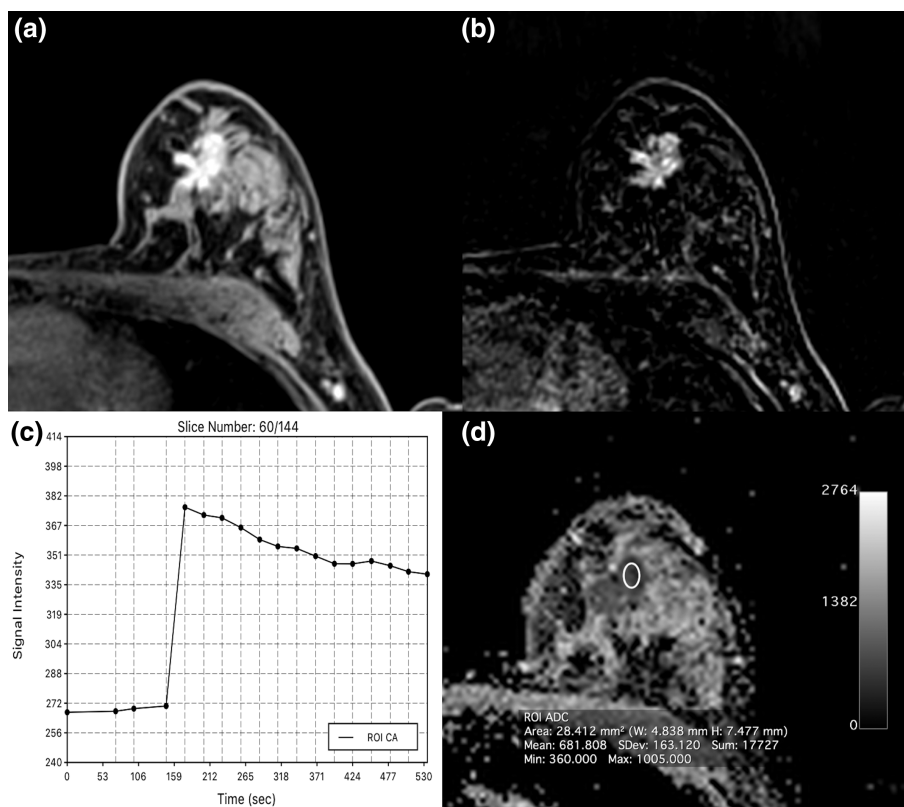


FIGURE 3: Invasive ductal carcinoma (IDC) grade 3 retroareolar in the left breast in a 47-year-old woman: On DCE-MRI there is a 23-mm (A) irregularly shaped and partly spiculated mass with (B) an initial fast heterogeneous contrast enhancement followed by a washout and (C) decreased ADC values ($0.0681 \times 10^{-3} \text{ mm}^2/\text{s}$) evident.

determined that ADCmean on DWI; and margins, initial enhancement, and enhancement in the delayed phase on DCE-MRI were significantly associated with breast cancer diagnosis.

Following these findings, mpMRI Model 2 incorporated ADCmean (continuous form); and margins, initial enhancement, and delayed enhancement on DCE-MRI. Model 2 exhibited a slightly better diagnostic accuracy compared with mpModel 1 (AUC = 0.971, $P = 0.063$ vs. AUC = 0.952, $P = 0.305$ [Fig. 2], respectively). As the ADCmean decreased, the likelihood of a lesion being malignant increased. With each unit ($10^{-3} \text{ mm}^2/\text{sec}$) increase in ADCmean, the odds of the lesion being cancer decreased significantly (CI = 0.016 0.002–0.151), $P = 0.0003$). Lesions with irregular or spiculated margins presented with an almost 5-fold risk of being malignant (OR = 4.979; CI = 1.886–13.145) than lesions with persistent enhancement ($P = 0.0012$). Lesions with plateau or washout kinetic curves had a 3.7-fold risk of being malignant (OR = 3.687; CI = 1.440–9.446) than lesions with persistent enhancement ($P = 0.0003$). In addition, in the mpMRI model including ADCmean as a continuous variable, an initial fast enhancement was also found to be associated with increased odds of being malignant as opposed to a slow/medium initial enhancement (OR = 12.67; CI = 1.094–146.784; $P = 0.0422$) (Figs. 3–4).

Discussion

We show that an mpMRI model for breast cancer diagnosis with a high diagnostic accuracy incorporates quantitative and qualitative variables from both DCE-MRI and DWI. In particular, models using ACR BI-RADS descriptors of margins and enhancement kinetics on DCE-MRI, and ADCmean with DWI either using a cutoff value ($\leq 1.25 \times 10^{-3} \text{ mm}^2/\text{sec}$) or as a continuous variable were strongly associated with breast cancer diagnosis (AUC 0.95 and 0.971, respectively). Conventional T_2 -weighted imaging did not significantly contribute to breast cancer diagnosis.

The MRI BI-RADS lexicon recommends that in the typical breast MRI protocol, T_2 -weighted sequences are acquired along with DCE-MRI. Nevertheless, there has been growing evidence for the diagnostic value of mpMRI using DCE-MRI and DWI with ADC mapping. Given the potential of this mpMRI approach, the incremental value of a protocol including T_2 -weighted imaging, DCE-MRI, and DWI using ADC mapping, using descriptors conforming to the MRI BI-RADS lexicon needs to be addressed. Until then, it remains unclear what needs to be included in a standard MRI protocol for the most accurate breast cancer diagnosis.

We designed this study to close this gap in knowledge and to clarify which descriptors from DCE-MRI, DWI, and T_2 -weighted imaging are most strongly associated with the

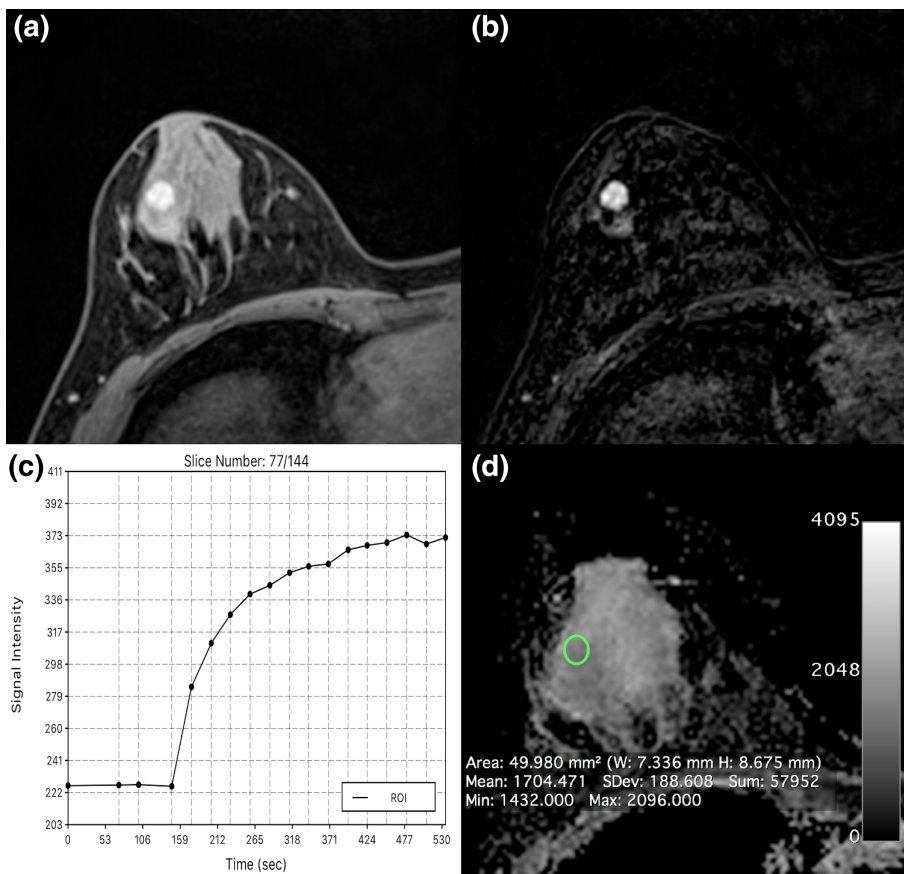


FIGURE 4: Fibroadenoma centrolateral in the left breast in a 24-year-old woman: On DCE-MRI there is a 10-mm (A) circumscribed mass with (B) an initial medium/delayed persistent homogeneous contrast enhancement with ADC values above the cutoff for malignancy ($1.704 \times 10^{-3} \text{ mm}^2/\text{s}$) evident.

diagnosis of breast cancer. We analyzed the contribution of the individual BI-RADS descriptors for DCE-MRI (type of enhancement, shape, margin, internal enhancement pattern/characteristics, enhancement kinetics) and T₂-weighted imaging (signal intensity, peritumoral edema), as well as different ADC metrics (ADC_{mean}, min, max) on DWI, and we developed mpMRI models for breast cancer diagnosis. In breast imaging, such models based on MRI have already been shown to be beneficial for improved lesion characterization and staging. Knuttel et al presented a model that incorporated DCE-MRI and the amount of fibroglandular tissue for the prediction of extensive ductal carcinoma in situ around early-stage invasive breast cancer.²⁵ Rahbar et al developed a model incorporating DCE-MRI and DWI descriptors that differentiated high nuclear grade from nonhigh nuclear grade ductal carcinoma in situ.²⁶ Cheeney et al investigated whether DWI could assist in determining which high-risk lesions previously identified on DCE-MRI and diagnosed on core needle biopsy would be upgraded to malignancy at surgical excision, showing that ADC_{mean} and maximum lesion size on DCE-MRI held promise.²⁷

Our models show that irregular or spiculated lesions, lesion with initial medium/fast enhancement, and lower ADC_{mean} values are significantly more likely to be malignant.

Furthermore, adding DWI with ADC mapping to the standard DCE-MRI protocol improved diagnostic accuracy, whereas adding T₂-weighted imaging did not, suggesting that T₂-weighted imaging may be omitted and replaced by the information afforded with DWI. Numerous studies have shown that another benefit of mpMRI with DCE-MRI and DWI is in decreasing unnecessary breast biopsies of benign breast tumors prompted by routine MRIs.^{15–18,28} In the current study we also demonstrate that mpMRI outperforms routine MRI alone, which achieved an AUC 0.8182 as compared to AUC 0.95 and 0.971, respectively, and thus would have obviated unnecessary breast biopsies in benign lesions. This is of particular interest, as abbreviated as well as ultrafast dynamic imaging protocols have been evaluated and there is discussion whether to offer MRI screening to women at average risk of breast cancer in addition to those with increased risk.^{3,29–32} Moreover, the additional information gained by DWI with ADC mapping might be used during MRI guidance for enhanced targeting to biopsy the most aggressive portion of a lesion, thereby decreasing sampling error.

While on univariate analysis we found that patient age, lesion laterality, different BI-RADS descriptors for DCE-MRI (mass shape, margin and internal enhancement characteristics, initial and delayed phase enhancement, T₂-weighted peritumoral edema), and different DWI variables (ADC_{mean}, max,

min, DWI signal intensity on b50) were significant predictors of breast cancer, multivariate logistic regression analysis yielded two mpMRI models for the most accurate breast cancer diagnosis that included only qualitative (margins) and quantitative (initial and delayed enhancement, ADCmean) features from DCE-MRI and DWI. In the literature, different ADC cutoff values have been proposed to distinguish malignant from benign lesions, ranging from $0.9\text{--}1.76 \times 10^{-3} \text{ mm}^2/\text{sec}$, while a meta-analysis of 12 articles recommended a threshold of $1.23 \times 10^{-3} \text{ mm}^2/\text{sec}$.¹¹ We explored different ADCmetrics, ie, mean, min, and max, and used both a cutoff ADCmean value and ADCmean as a continuous variable for the mpMRI model development. In both mpMRI models, ADCmean remained a significant predictor for malignancy with an AUC of 0.952 (binary) and 0.971 (continuous), respectively.

As previously mentioned, the T₂-weighted imaging variables were not included in the final model. Although prior studies indicate that assessing the T₂-weighted signal intensity of a lesion relative to a tissue of reference improves diagnostic accuracy,^{33–35} in this study the signal intensity of a lesion on T₂-weighted imaging did not contribute significantly breast cancer diagnosis. Early results by Kuhl et al³³ are line with this finding and have shown that high T₂-weighted signal intensity should be used to confirm benignity as indicated by DCE-MRI than rule out cancer. Several more recent studies have also demonstrated that breast cancers, especially triple-negative breast cancers, may present with variable signal intensities on T₂-weighted imaging,³⁶ which is further substantiated by our results. Several studies have also shown that the presence of a peritumoral edema is indicative of malignancy^{37,38} and is associated with breast cancer with an unfavorable prognosis.^{39,40} Although the presence of a peritumoral edema was significant on univariate analysis, this imaging feature was not included in the final mpMRI model and thus T₂-weighted imaging did not have a contribution to the mpMRI model for breast cancer diagnosis.

Our study is limited by the relatively small number of pure ductal carcinoma in situ and invasive lobular carcinoma compared with invasive ductal cancers, limiting the generalization of the findings in these smaller subgroups. In addition, this is a retrospective study, which inherently could have covariates that we have not accounted for. This study was also conducted at a single tertiary center institution, and the interpretations were performed by experienced breast fellowship-trained radiologists, potentially making it difficult to extrapolate to community practice. A limitation of this study is that we did not estimate ROC curves from independent datasets; hence, the ROC curves can be an overestimate. The models will therefore be prospectively tested in further studies.

In conclusion, mpMRI with DCE-MRI and DWI with ADC mapping enables an accurate breast cancer diagnosis. Models using quantitative and qualitative descriptors from

DCE-MRI and DWI identifies breast cancer with a high diagnostic accuracy. Additional T₂-weighted imaging does not significantly contribute to breast cancer diagnosis.

Acknowledgment

The authors acknowledge the support in article writing and editing from Joanne Chin.

Contract grant sponsor: Austrian Nationalbank ‘Jubiläumfond’; Contract grant numbers: 16219, 15082; Contract grant sponsor: 2020 - Research and Innovation Framework Programme PHC-11-2015; Contract grant number: 667211-2; Contract grant sponsor: Novomed Austria; Contract grant sponsor: Medicor Austria; Contract grant sponsor: Guerbet France; Contract grant sponsor: NIH/NCI Cancer Center; Contract grant number: P30 CA008748.

References

- Mann RM, Balleyguier C, Baltzer PA, et al. Breast MRI: EUSOBI recommendations for women’s information. *Eur Radiol* 2015;25:3669–3678.
- Riedl CC, Luft N, Bernhart C, et al. Triple-modality screening trial for familial breast cancer underlines the importance of magnetic resonance imaging and questions the role of mammography and ultrasound regardless of patient mutation status, age, and breast density. *J Clin Oncol* 2015;33:1128–1135.
- Kuhl CK, Strobel K, Bieling H, Leutner C, Schild HH, Schrading S. Supplemental breast MR imaging screening of women with average risk of breast cancer. *Radiology* 2017;283:361–370.
- Krammer J, Pinker-Domenig K, Robson ME, et al. Breast cancer detection and tumor characteristics in BRCA1 and BRCA2 mutation carriers. *Breast Cancer Res Treat* 2017;163:565–571.
- Zhang L, Tang M, Min Z, Lu J, Lei X, Zhang X. Accuracy of combined dynamic contrast-enhanced magnetic resonance imaging and diffusion-weighted imaging for breast cancer detection: a meta-analysis. *Acta Radiol* 2016;57:651–660.
- Mann RM, Balleyguier C, Baltzer PA, et al. Breast MRI: EUSOBI recommendations for women’s information. *Eur Radiol* 2015;25:3669–3678.
- Ouwerkerk R, Jacobs MA, Macura KJ, et al. Elevated tissue sodium concentration in malignant breast lesions detected with non-invasive ²³Na MRI. *Breast Cancer Res Treat* 2007;106:151–160.
- Zaric O, Pinker K, Zbyn S, et al. Quantitative sodium MR imaging at 7 T: Initial results and comparison with diffusion-weighted imaging in patients with breast tumors. *Radiology* 2016;280:39–48.
- Baltzer PA, Dietzel M. Breast lesions: diagnosis by using proton MR spectroscopy at 1.5 and 3.0 T—systematic review and meta-analysis. *Radiology* 2013;267:735–746.
- Dorrius MD, Dijkstra H, Oudkerk M, Sijens PE. Effect of b value and pre-admission of contrast on diagnostic accuracy of 1.5-T breast DWI: a systematic review and meta-analysis. *Eur Radiol* 2014;24:2835–2847.
- Partridge SC, McDonald ES. Diffusion weighted magnetic resonance imaging of the breast: protocol optimization, interpretation, and clinical applications. *Magn Reson Imaging Clin N Am* 2013;21:601–624.
- Chen X, Li WL, Zhang YL, Wu Q, Guo YM, Bai ZL. Meta-analysis of quantitative diffusion-weighted MR imaging in the differential diagnosis of breast lesions. *BMC Cancer* 2010;10:693.
- Marino MA, Helbich T, Baltzer P, Pinker-Domenig K. Multiparametric MRI of the breast: A review. *J Magn Reson Imaging* 2018;47:301–315.
- lima M, Le Bihan D. Clinical intravoxel incoherent motion and diffusion MR imaging: Past, present, and future. *Radiology* 2016;278:13–32.

15. Partridge SC, DeMartini WB, Kurland BF, Eby PR, White SW, Lehman CD. Quantitative diffusion-weighted imaging as an adjunct to conventional breast MRI for improved positive predictive value. *AJR Am J Roentgenol* 2009;193:1716–1722.
16. Baltzer A, Dietzel M, Kaiser CG, Baltzer PA. Combined reading of contrast enhanced and diffusion weighted magnetic resonance imaging by using a simple sum score. *Eur Radiol* 2016;26:884–891.
17. Pinker K, Bickel H, Helbich TH, et al. Combined contrast-enhanced magnetic resonance and diffusion-weighted imaging reading adapted to the “Breast Imaging Reporting and Data System” for multiparametric 3-T imaging of breast lesions. *Eur Radiol* 2013;23:1791–1802.
18. El Khouli RH, Jacobs MA, Mezban SD, et al. Diffusion-weighted imaging improves the diagnostic accuracy of conventional 3.0-T breast MR imaging. *Radiology* 2010;256:64–73.
19. Pinker K, Moy L, Sutton EJ, et al. Diffusion-weighted imaging with apparent diffusion coefficient mapping for breast cancer detection as a stand-alone parameter: comparison with dynamic contrast-enhanced and multiparametric magnetic resonance imaging. *Invest Radiol* 2018 [Epub ahead of print].
20. D’Orsi CJ, Sickles EA, Mendelson EB, et al. *ACR BI-RADS Atlas, Breast Imaging Reporting and Data System*. Reston, VA: American College of Radiology; 2013.
21. Mann RM, Kuhl CK, Kinkel K, Boetes C. Breast MRI: guidelines from the European Society of Breast Imaging. *Eur Radiol* 2008;18:1307–1318.
22. Rosset A, Spadola L, Ratib O. OsiriX: An open-source software for navigating in multidimensional DICOM images. *J Digit Imaging* 2004;17:205–216.
23. Bogner W, Gruber S, Pinker K, et al. Diffusion-weighted MR for differentiation of breast lesions at 3.0 T: how does selection of diffusion protocols affect diagnosis? *Radiology* 2009;253:341–351.
24. DeLong ER, DeLong DM, Clarke-Pearson DL. Comparing the areas under two or more correlated receiver operating characteristic curves: a non-parametric approach. *Biometrics* 1988;44:837–845.
25. Knuttel FM, van der Velden BH, Loo CE, et al. Prediction model for extensive ductal carcinoma in situ around early-stage invasive breast cancer. *Invest Radiol* 2016;51:462–468.
26. Rahbar H, Partridge SC, Demartini WB, et al. In vivo assessment of ductal carcinoma in situ grade: a model incorporating dynamic contrast-enhanced and diffusion-weighted breast MR imaging parameters. *Radiology* 2012;263:374–382.
27. Cheeney S, Rahbar H, Dontchos BN, Javid SH, Rendi MH, Partridge SC. Apparent diffusion coefficient values may help predict which MRI-detected high-risk breast lesions will upgrade at surgical excision. *J Magn Reson Imaging* 2017;46:1028–1036.
28. Pinker K, Baltzer P, Bogner W, et al. Multiparametric MR imaging with high-resolution dynamic contrast-enhanced and diffusion-weighted imaging at 7 T improves the assessment of breast tumors: a feasibility study. *Radiology* 2015;276:360–370.
29. Kuhl CK, Schrading S, Stobel K, Schild HH, Hilgers RD, Bieling HB. Abbreviated breast magnetic resonance imaging (MRI): first postcontrast subtracted images and maximum-intensity projection—a novel approach to breast cancer screening with MRI. *J Clin Oncol* 2014;32:2304–2310.
30. Chen SQ, Huang M, Shen YY, Liu CL, Xu CX. Application of abbreviated protocol of magnetic resonance imaging for breast cancer screening in dense breast tissue. *Acad Radiol* 2017;24:316–320.
31. Grimm LJ, Soo MS, Yoon S, Kim C, Ghate SV, Johnson KS. Abbreviated screening protocol for breast MRI: a feasibility study. *Acad Radiol* 2015;22:1157–1162.
32. Kuhl CK. Abbreviated breast MRI for screening women with dense breast: The EA1141 Trial. *Br J Radiol* 2017:20170441.
33. Kuhl CK, Klaschik S, Mielcarek P, Gieseke J, Wardelmann E, Schild HH. Do T2-weighted pulse sequences help with the differential diagnosis of enhancing lesions in dynamic breast MRI? *J Magn Reson Imaging* 1999;9:187–196.
34. Moran CJ, Hargreaves BA, Saranathan M, et al. 3D T2-weighted spin echo imaging in the breast. *J Magn Reson Imaging* 2014;39:332–338.
35. Arponen O, Masarwah A, Sutela A, et al. Incidentally detected enhancing lesions found in breast MRI: analysis of apparent diffusion coefficient and T2 signal intensity significantly improves specificity. *Eur Radiol* 2016;26:4361–4370.
36. Angelini G, Marini C, Iaconi C, et al. Magnetic resonance (MR) features in triple negative breast cancer (TNBC) vs receptor positive cancer (nTNBC). *Clin Imaging* 2017;49:12–16.
37. Uematsu T. Focal breast edema associated with malignancy on T2-weighted images of breast MRI: peritumoral edema, prepectoral edema, and subcutaneous edema. *Breast Cancer* 2015;22:66–70.
38. Baltzer PA, Yang F, Dietzel M, et al. Sensitivity and specificity of unilateral edema on T2w-TSE sequences in MR-Mammography considering 974 histologically verified lesions. *Breast J* 2010;16:233–239.
39. Bae MS, Shin SU, Ryu HS, et al. Pretreatment MR imaging features of triple-negative breast cancer: association with response to neoadjuvant chemotherapy and recurrence-free survival. *Radiology* 2016;281:392–400.
40. Song SE, Shin SU, Moon HG, Ryu HS, Kim K, Moon WK. MR imaging features associated with distant metastasis-free survival of patients with invasive breast cancer: a case-control study. *Breast Cancer Res Treat* 2017;162:559–569.